Methane Hydrate Nonstoichiometry and Phase Diagram

Zhongxin Huo, Keith Hester, and E. Dendy Sloan, Jr.
Center for Hydrate Research, Colorado School of Mines, Golden, CO 80401

Kelly T. Miller
Dept. of Metallurgical and Materials Engineering, Colorado School of Mines, Golden, CO 80401

A previous study discovered that, when formed from different ethylene oxide (EO) feed solutions, hydrates had different small-cage occupancies with essentially total occupation of the large cavities of sI hydrate. An $EO + H_2O$ isobaric phase diagram was proposed with a solid solution range to explain this phenomenon. Since methane and CO_2 also occupy both small cages and large cages of sI hydrate, new phase diagrams were proposed which allowed the methane or CO_2 hydrate composition to vary as a function of feed composition at fixed p-T conditions. Raman spectroscopy experiments now show that $H_2O + CH_4$ hydrates formed at the vapor−liquid interface have a different composition than dendrites growing into the water below the interface. Interfacial hydrates were typical laboratory samples formed with excess gas, while dendrites coexisted with excess water and were similar to seafloor hydrate. Integrated peak intensities were used to calculate relative cage occupancies in Raman data analysis. Interfacial hydrates had an average of 95.4% small cages occupied at 30 MPa and 275.15 K, while dendrite hydrates had only 82.8% small-cage occupancy at the same conditions. This result suggests that hydrates in the ocean floor may have lower methane concentrations than hydrates formed under normal laboratory conditions at the same pressure and temperature.

Introduction

A previous diffraction study showed that ethylene oxide (EO) sI lattice parameters were smaller for hydrates formed from EO-lean solutions ($a = 11.987$ Å) than those from EO-rich solutions ($a = 12.022$ Å) (Huo et al., 2002). As shown in Figure 1, this phenomenon was explained by a new isobaric $EO + H_2O$ *T-x* phase diagram with a solid solution range. When hydrates were formed from an EO-lean solution (such as anywhere along line *AB* at *T′*), the hydrates had fewer small cages occupied by EO guests, and thus a smaller lattice parameter. In contrast, hydrates formed from an EO-rich solution (such as anywhere along line *CD* at *T′*) had more small cages occupied, and thus a larger lattice parameter. In the single hydrate phase region, the lattice parameter increased monotonically with increasing EO composition. This explanation was validated by Raman spectroscopy measurements on cage occupation and agreed well with density measurements by Glew and Rath (1966).

Since pure guests of methane and CO_2 each also occupy the small cages (and the large cages as well) of sI hydrate, similar compositional changes may exist if the overall system composition was varied. As shown in Figure 2, a $CH_4 + H_2O$ *T-x* phase diagram with a solid solution range was proposed based on the EO hydrate work and the original $CH_4 + H_2O$ isobaric ($p \approx 5$ MPa) *T-x* diagram by Kobayashi and Katz (1949). Kobayashi and Katz had proposed a vertical line for the hydrate compositions, which discounts hydrate nonstoichiometry. However, hydrates are known to be nonstoichiometric, because not every water cage needs to be filled with a guest molecule (Sloan, 1998, p. 55).

A hypothesis from the previous study was that the amount of methane in naturally occurring hydrates (seafloor and per-

Correspondence concerning this article should be addressed to E. D. Sloan, Jr.

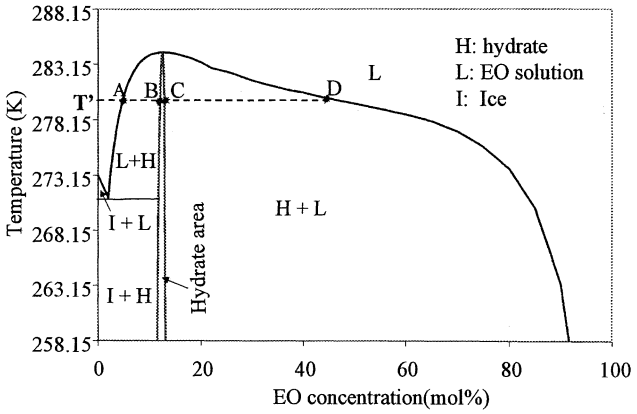

Figure 1. EO *T-x* phase diagram with solid solution range ($p = 0.1$ MPa).

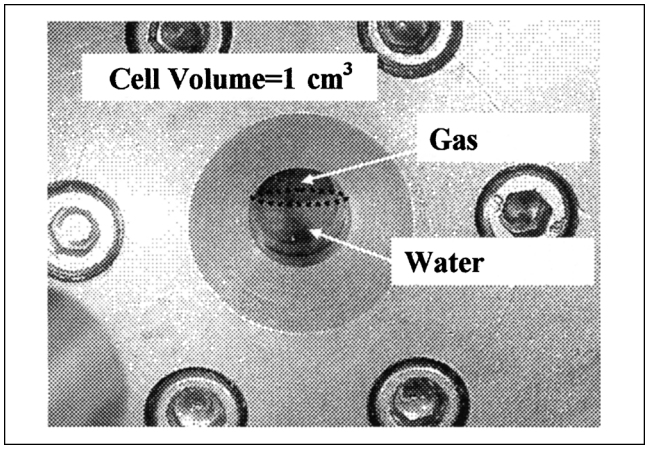

Figure 3. Raman cell.

mafrost) might be less than predicted amounts based upon lab conditions. Hydrates in nature typically form from CH saturated water (Hyndman et al., 1992). Due to the low solubility of methane in aqueous phase, however, laboratory-made methane hydrates are typically formed at the water–gas interface using the method of Stern et al. (1996) with excess free gas.

In a recent study, Subramanian (2000, p. 257) observed both interfacial and dendrite methane hydrate growth in a Raman cell with a high driving force (> 10°C). The interfacial hydrates were in contact with the methane-gas phase, while the dendrites grew from the bottom of the interfacial hydrate layer, extending into the aqueous phase, where the solid hydrate interface blocked bulk phase contact. While the interfacial hydrates were in equilibrium with excess gas, dendrite hydrates formed and equilibrated with excess water without free gas, similar to naturally occurring hydrates. Since Raman spectroscopy can measure relative cage occupancies (Subramanian, 2000, chap. 5; Subramanian et al., 2000), any significant difference in hydrate composition between interfacial hydrates and dendrite hydrates can be quantified and used to estimate the composition in naturally occurring hydrates and in laboratory-prepared hydrates.

This work measured both interfacial- and dendrite-hydrate cage occupancies by Raman spectroscopy. Hydrate composition predictions as a function of overall system composition were compared to Raman measurements.

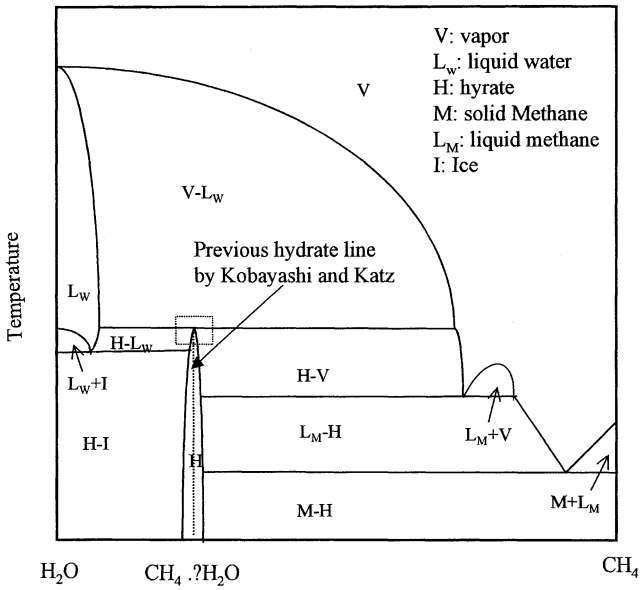

Figure 2. Proposed CH_4-H_2O *T-x* phase diagram with solid solution range ($p \approx 5$ MPa).

Dashed box region shown in Figure 8.

Apparatus and Experimental Procedures

A Renishaw Inc. MK III Raman spectrometer was used, utilizing a 30-mW argon-ion laser emitting green light at a wavelength of 514.53 nm as an excitation source (Subramanian, 2000, p. 32). The light was transported through a 50-μm optic-fiber cable to the probe and was focused on the sample via a 5X objective lens.

Backscattered light was filtered using a 2,400 grooves/mm grating. The spectrometer was calibrated using the emission lines from neon, with an accuracy of 0.3 cm^{-1}, while the spectral resolution was 4.5 cm^{-1}. Raman spectra were analyzed using GRAMS/32 software from Galactic Industries Corporation.

Figure 3 shows the Raman hydrate formation cell. The dashed ellipse is at the methane–water interface. Methane gas was first charged before water was input via a Ruska hand pump to increase the pressure to 30 MPa. The pressure was detected by a Sensotec pressure transducer (model: TJE/743-06; accuracy: $\pm 0.1\%$) and monitored by a Sensotec reader (model: 060-3147-01). The relative volume of water/gas in the cell was approximately 10:1. The cell was cooled to 275.15 K, and hydrate formation was monitored by a Sony AVC-D7 CCD camera combined with an Olympus SZ60 microscope.

As shown in Figure 4, shortly after the interfacial hydrates were formed, a significant number of needle-shaped hydrates (dendrites) grew into the aqueous phase, extending approximately 5 mm below the interface. Minor pressure drops (~ 0.3

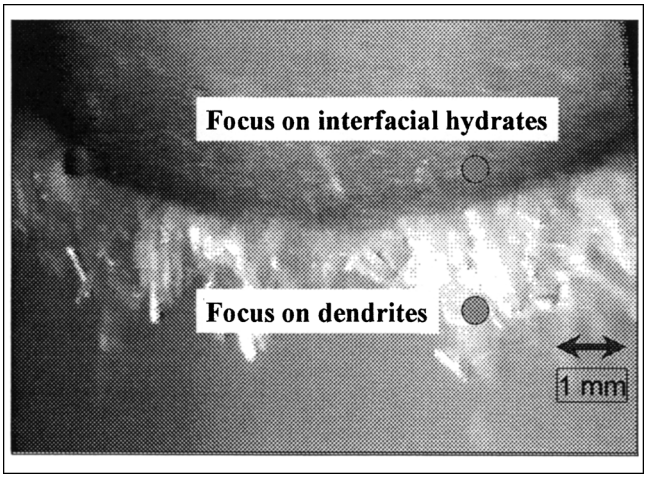

Figure 4. Interfacial and dendrite hydrates.

MPa) during hydrate formation were compensated by recharging the cell with water three times. The laser beam, approximately 0.5 mm in diameter, was focused on the interfacial and dendrite hydrates separately to obtain cage occupancy information. The spectra were collected for 400 s each over the range of 2,800 to 3,050 cm^{-1}, where contributions from the methane C–H bond vibration were found. Since dendrites were inside the bulk aqueous phase, some contribution from dissolved-methane may be present in the spectra. Similarly, because the interfacial hydrate layer was nonuniform and thin, gas contributions were always observed in these spectra. Free gas and dissolved methane contributions were removed in the data analysis, as shown below.

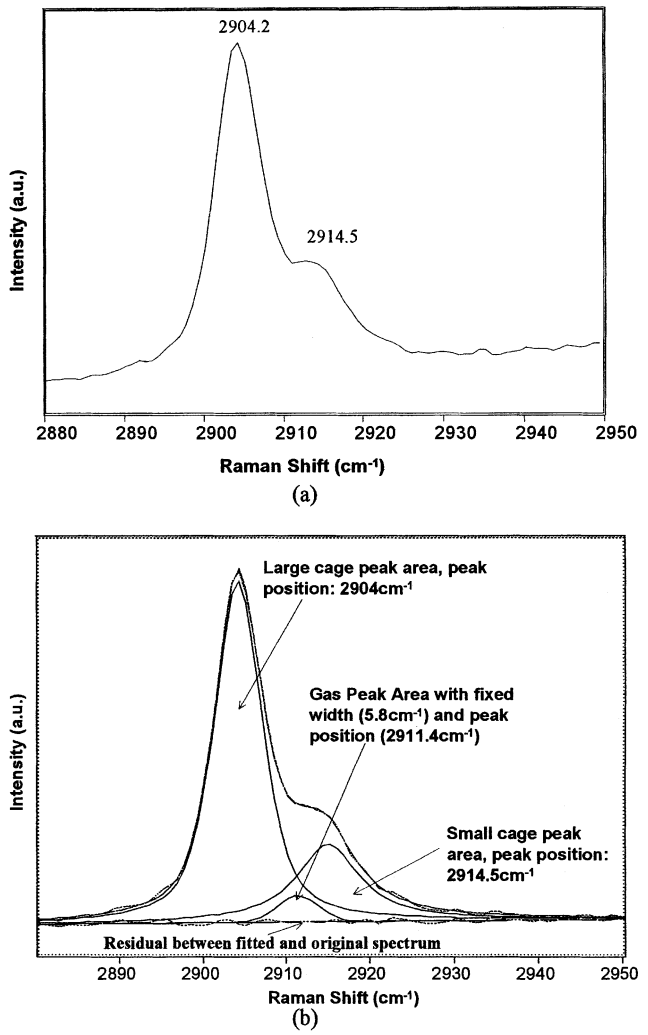

Figure 5. Data-processing procedures.

The spectra were processed by first subtracting water base line using the GRAMS/32 software. Since the small-cage and large-cage contributions (peaks) were overlapping, peaks were deconvoluted by a mixed Lorenzian–Gaussian method. Both the dissolved methane contribution in the dendrite-hydrate spectra and methane-gas contribution in interfacial-hydrate spectra were fitted with a fixed width and peak position (Jager, 2001, p. 137). Integral peak intensities of hydrate peaks in arbitrary units (a.u.) were used for relative cage occupancy calculations. Figure 5 illustrates this procedure using a sample interfacial-methane-hydrate spectrum taken at 30 MPa and 275.15 K. In Figure 5a, the peak at ~ 2,904 cm^{-1} is the methane contribution of the large cage, while the peak at ~ 2,914.5 cm^{-1} is the contribution of the small cage. The upwardly sloping base line in the unprocessed spectrum is the water contribution. In processing this spectrum, the water contribution was first subtracted by the GRAMS/32 software to obtain a flat base line. As shown in Figure 5b, peaks at 2,904, 2,911.4 and 2,914.5 cm^{-1} were designated as large-cage, gas, and small-cage contributions, respectively. During the Lorenzian–Gaussian peak deconvolution, both the peak position and the peak width of the hydrate contributions were allowed to vary, but the gas contribution was fixed in peak position and width. As shown in Figure 5b, the original and fitted lines coincided, as indicated by the small residual. The relative cage occupancy of the large and small cages was then calculated as

$$\frac{\theta_l}{\theta_s} = \left(\frac{A_l}{A_s}\right)/3, \tag{1}$$

where θ_1 and θ_s are large- and small-cage occupancies, and A_1 and A_s are the integral intensities of the contribution of methane in the large and small cages, fitted by the GRAMS/32 software. In the equation, the "3" accounts for the fact that there are three times as many large cages as small cages in a structure I unit cell. Complete large-cage occupancy was assumed so that small-cage occupancies could be calculated. Complete large-cage occupancy for sI hydrate has been observed by different researchers (Handa, 1986; Udachin et al., 2002) and is a prerequisite for hydrate stability (Dyadin et al., 1991).

Results

As shown in Figure 6, the methane-gas spectrum was collected prior to hydrate formation at 30 MPa and 275.15 K. The dissolved methane spectrum was also collected before hydrate formation, while the water base line was collected in a separate run without methane gas. At 30 MPa and 275.15 K, methane gas was found to have a contribution at 2,911.4

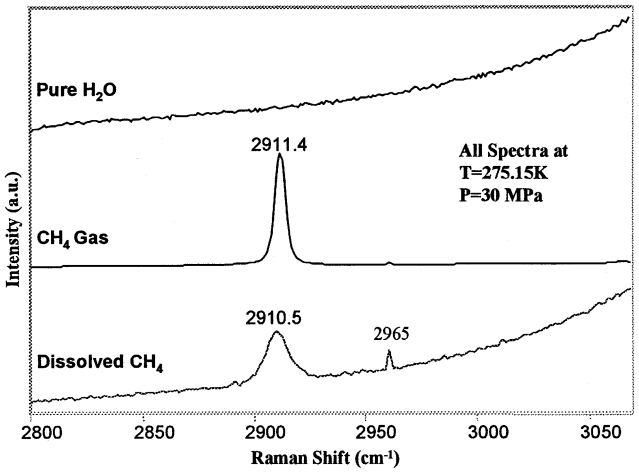

Figure 6. Contributions of water, methane gas, and dissolved methane.

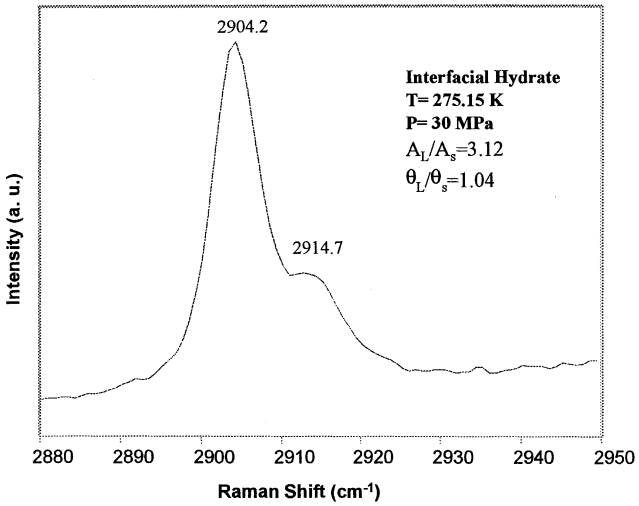

Figure 7. Interfacial hydrate spectrum.

cm^{-1} with a full width at half maximum (FWHM) of 5.8 cm^{-1}, while dissolved methane had a contribution at 2910.5 cm^{-1} with a FWHM of 11.8 cm^{-1}. The minor peak at 2,965 cm^{-1} on the dissolved-methane spectrum was caused by a CCD camera defect and was ignored in data analysis (Jager, 2001, p. 153).

Figure 7 shows a typical 400-s-collection-time interfacial-hydrate spectrum with a visible contribution from water. Twenty such spectra were collected for accurate peak-intensity calculations. Following the procedures of the previous section, by subtracting the water contribution and deconvoluting peaks using the Lorenzian–Gaussian method, the average large/small cage occupancy ratio was found to be 1.041, indicating that the average small-cage occupancy was approximately 96.1% at the interface, if large-cage full occupation was assumed. As shown in Table 1, this result was very reproducible, and the standard deviation in small-cage occupancy from all 20 spectra was 3%. As shown in Figure 8, these measurements did not agree well with previous work by Jager (2001, p. 138) as compared to predictions, but the discrepancy was insignificant compared to error.

Figure 9 is a typical dendrite-hydrate spectrum that also has a total collection time of 400 s. Thirteen such spectra were collected during the same period the interfacial-hydrate spectra were collected. In deconvoluting dendrite-hydrate spectra, the dissolved-methane (instead of a methane gas) contribution was considered with fixed width and peak position. The average large/small cage occupancy ratio was found

Table 1. Interfacial Hydrate Composition Measurements

Large Peak Area (A_L)	Small Peak Area (A_S)	Occ. Ratio	θ_s*	mol % C1*	θ_s**	mol % C1**	Date Measured
306,152	97,861	1.04	0.9512	14.61	0.9589	14.68	10/20/2001
299,985	99,948	1.00	0.9915	14.74	0.9995	14.81	10/20/2001
292,079	97,255	1.00	0.9909	14.74	0.9989	14.81	10/20/2001
302,437	92,416	1.09	0.9094	14.47	0.9167	14.55	10/20/2001
301,999	100,525	1.00	0.9906	14.73	0.9986	14.81	10/30/2001
302,906	96,226	1.05	0.9454	14.59	0.9530	14.66	10/30/2001
293,813	92,128	1.06	0.9332	14.55	0.9407	14.63	10/30/2001
299,183	93,478	1.07	0.9298	14.54	0.9373	14.62	10/30/2001
291,459	93,461	1.04	0.9543	14.62	0.9620	14.69	10/30/2001
300,627	95,369	1.05	0.9441	14.59	0.9517	14.66	11/05/2001
284,750	89,563	1.06	0.9361	14.56	0.9436	14.64	11/05/2001
279,592	91,636	1.02	0.9753	14.69	0.9832	14.76	11/05/2001
274,357	89,110	1.03	0.9666	14.66	0.9744	14.73	11/05/2001
276,317	84,770	1.09	0.9130	14.49	0.9204	14.56	11/05/2001
283,440	89,249	1.06	0.9370	14.56	0.9446	14.64	11/05/2001
275,463	91,408	1.00	0.9875	14.72	0.9955	14.80	11/05/2001
275,915	82,744	1.11	0.8925	14.42	0.8997	14.50	11/27/2001
266,200	86,830	1.02	0.9707	14.67	0.9785	14.75	11/27/2001
263,087	87,221	1.01	0.9866	14.72	0.9946	14.80	11/27/2001
256,504	83,456	1.02	0.9683	14.66	0.9761	14.74	11/27/2001
	Mean	1.041	0.954	14.62	0.961	14.69	
	St. Dev.	0.033	0.03	0.09	0.03	0.094	

*calculation based on CSMGem-predicted large-cage occupancy, 99.2%.
**Calculation based on complete large-cage occupancy assumption.

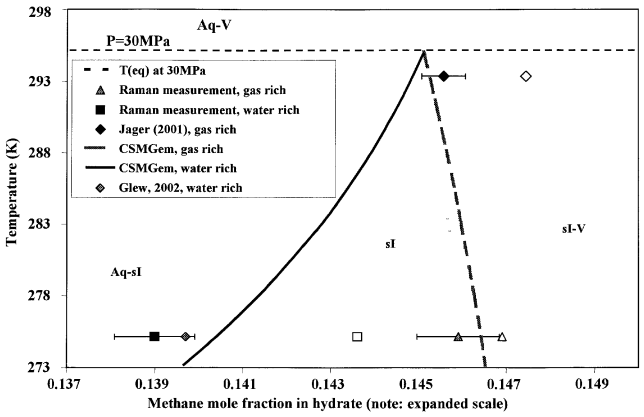

Figure 8. Expanded dashed box region of Figure 2: predicted and measured hydrate compositions.

Open symbols: complete large-cage occupancy assumed; filled symbols: large-cage occupancy predicted by CSMGem.

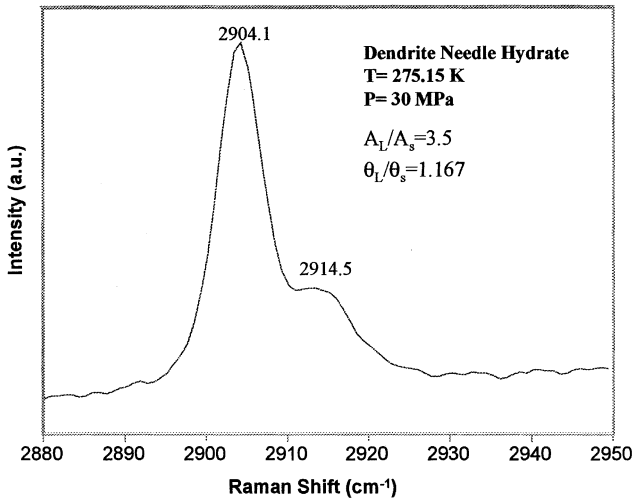

Figure 9. Dendrite hydrate spectrum.

to be 1.167, indicating that the average small-cage occupancy was approximately 85.8% in the dendrites, if full large-cage occupancy was assumed. As shown in Table 2, the standard deviation in small-cage occupancy from these 13 spectra was 3%. The contribution by either dissolved methane or methane gas was found to be negligible.

The dendrite hydrates in the Raman cell were allowed to stay at constant temperature (275.15 K) and pressure (30 MPa) for more than 30 days. Raman spectra were re-collected (as shown in Table 2) and no significant hydrate composition changes were observed. Nor was there any change in hydrate shape, indicating that dendrites were at or close to equilibrium. In a different study, Subramanian and Sloan (2002) observed needle growth with decreasing solution temperature and shrinkage with increasing solution temperature, indicating that the dendrite hydrates were at true two-phase (aqueous-hydrate) equilibrium.

Discussion

Because single-phase regions are more familiar to metallurgists and material scientists (Massalski, et al., 1990), a few words may be helpful regarding this somewhat unusual phenomenon, in view of the phase diagram of Figure 2. First, the single-phase hydrate region is not homogenous, but has varying compositions with temperature, pressure, and particularly composition. Thus, in order to specify the state of the single-phase region by the phase rule for two components (methane and water) and one hydrate phase, three intensive variables are required (such as the isobaric pressure, temperature, and hydrate phase composition).

When scientists and engineers see an area on a phase diagram such as Figure 2, they are sometimes tempted to apply the "Inverse Lever Rule" (Bett et al., 1975) to determine phase amounts, just as they would in any of the two-phase regions of the diagram, which have two degrees of freedom. However, due to the additional intensive variable in the single-phase hydrate-phase area, the Inverse Lever Rule does

Table 2. Dendrite Hydrate Composition Measurements

Large Peak Area (A_L)	Small Peak Area (A_s)	Occ. Ratio	θ_s*	mol % C1*	θ_s**	mol % C1**	Date Measured
130,024	37,291	1.16	0.83	13.90	0.86	14.37	10/20/2001
129,073	36,840	1.17	0.83	13.90	0.86	14.36	10/20/2001
298,781	88,535	1.12	0.86	13.99	0.89	14.46	10/23/2001
328,404	91,505	1.20	0.81	13.84	0.84	14.29	10/30/2001
421,531	124,677	1.13	0.86	13.99	0.89	14.46	10/30/2001
320,356	94,806	1.13	0.86	13.99	0.89	14.46	10/30/2001
377,174	104,628	1.20	0.80	13.81	0.83	14.28	10/31/2001
165,762	47,835	1.16	0.84	13.93	0.87	14.39	11/01/2001
591,084	166,742	1.18	0.82	13.87	0.85	14.33	11/28/2001
298,382	80,505	1.24	0.78	13.75	0.81	14.21	11/28/2001
421,481	127,517	1.10	0.88	14.06	0.91	14.52	11/28/2001
381,591	107,926	1.18	0.82	13.87	0.85	14.33	11/28/2001
380,327	105,046	1.21	0.80	13.81	0.83	14.27	11/28/2001
	Mean	1.167	0.828	13.901	0.858	14.365	
	St. Dev.	0.039	0.028	0.089	0.029	0.091	

*Calculation based on CSMGem-predicted large-cage occupancy, 96.3%.
**Calculation based on complete large-cage occupancy assumption.

not apply in the single-phase region, and it is incorrect to suggest that any point in the hydrate region is a mixture of two hydrate compositions. Rather, the state of the single-phase region is fixed at that point of composition, temperature, and pressure.

Second, it is important to note that the nonstoichiometry shown in Figures 1 and 2 may be in part responsible for the wide range of hydration numbers for methane hydrate (Sloan, 1998, p. 223). For example, at a lower initial feed (or overall) composition at a high temperature in Figure 2, the hydration number can be measurably less than a higher hydrate composition, which would result from a higher overall feed composition. In the past, these differing hydration numbers had been wholly attributed to experimental inaccuracies, such as might be obtained with water occlusion into a hydrate mass.

A Gibbs free-energy minimization program (CSMGem; Ballard and Sloan, 2002a,b) enabled the prediction of the methane-hydrate solid-solution range shown in Figure 2. The region in the dashed box in Figure 2 is of particular interest because it is the hydrate composition range where both laboratory-made and naturally occurring methane hydrates are formed. Figure 8 is the detailed phase diagram for the dashed box region in Figure 2 showing predicted and measured hydrate compositions, with an expanded abscissa scale.

In the extended scale of Figure 8, equilibrium hydrate compositions were predicted with the lean phase fully consumed. For example, the solid line marked "CSMGem, water rich" was the predicted hydrate composition with a final water/hydrate two-phase equilibrium, while the dashed line marked "CSMGem, gas rich" was the prediction with a final hydrate-methane vapor two-phase equilibrium. To the left of the water-rich line is the aqueous-hydrate two-phase region; to the right of the gas-rich line is the gas-hydrate two-phase region; in between these two lines is the single hydrate phase region (the solid solution range).

The prediction indicated that hydrates formed under water-rich conditions have approximately 4% less methane encaged than hydrates formed under gas-rich conditions at 275.15 K and 30 MPa, while the Raman measurements showed that the difference was approximately 2.6% at the same conditions. The predictions matched the measurements within a mole fraction of 0.003. As also shown in this figure on expanded scale, the prediction agrees within 0.001 mole-fraction result of Glew (2002).

However, the complete large-cage occupancy assumption in this work was based on historical literature evaluations, most of which were concerned with guests that occupied the large cage only (Handa, 1986; Udachin et al., 2002). In methane hydrates, since the hydrate stability is enhanced by small-cage occupancy, complete large-cage occupancy may no longer be a necessity for hydrates to be stable. As predicted by CSMGem, at 2°C and 30 MPa, 99.2% and 96.3% of the large cages were occupied for hydrates in equilibrium with vapor and the aqueous phase, respectively, and with 98.5% occupation of the large cage for Jager's (2001) three phase (H-V-Aq) condition. As shown in Figure 8, if these values are used to calculate the hydrate composition in Raman spectroscopy, the measurements and the predictions matched within 0.001 mole fraction. The discrepancy between the current measurements and Jager's (2001) was also eliminated.

It has been estimated that naturally occurring methane hydrates in seafloor sediments and permafrost have more than twice the energy content of the combination of all other types of fossil-fuel deposits (Kvenvolden, 1988; Kvenvolden and Lorenson, 2001). A $2.6 \sim 4\%$ difference in hydrate composition is equivalent to $2.6 \sim 4 \times 10^{14}$ kg of methane in natural-gas hydrates, which is more than 500 years of natural gas consumption for the USA according to its 2001 consumption level (23 Tcf/yr; Economides et al., 2001).

Conclusions

This work quantified the compositional difference between interfacial methane hydrates and dendrites at 30 MPa and 275.15 K. The dendrites, which were coexisting with the aqueous solution, were found to have up to 12.6% lower small-cage occupancy. A prediction method matched this measured composition variation acceptably. This is an indication that naturally occurring hydrates contain less energy than estimations based on laboratory samples. The new phase diagram was used to provide a thermodynamic rationale for measured differences in hydration numbers, which had previously been attributed to experimental error.

Acknowledgments

The authors thank our industrial consortium members BP-Amoco, Chevron-Texaco, Department of Energy, Halliburton, Phillips, and Unocal for their financial support of this work. The authors thank the National Science Foundation for providing funding through Research Grant CTS-9634899 for the Raman apparatus. The authors thank Dr. Sivakumar Subramanian for his suggestions on dendrite hydrate measurements. The authors also thank Dr. David N. Glew, whose constancy in hydrate research led to many of the ideas in this manuscript, for his constructive critique of an earlier version.

Literature Cited

Ballard, A., and E. D. Sloan, "The Next Generation of Hydrate Prediction I. Hydrate Standard States and Incorporation of Spectroscopy," *Fluid Phase Equilib.*, 194–197, 371 (2002a).

Ballard, A., and E. D. Sloan, "The Next Generation of Hydrate Prediction: An Overview," *Proc. Int. Conf. on Gas Hydrates*, Yokohama, Japan, p. 307, (icgh@mori.mech.keio.ac.jp) (2002b).

Bett, K. E., J. S. Rowlinson, and G. Saville, *Thermodynamics for Chemical Engineers*, Athalone Press, Univ. of London, p. 349 (1975).

Dyadin, Y. A., I. V. Bondaryuk, and F. V. Zhurko, "Clathrate Hydrates at High Pressures," *Inclusion Compounds*, Vol. 5, J. L. Atwood, J. E. D. Davies, and D. D. MacNichol, eds., Oxford Univ. Press, Oxford, p. 213 (1991).

Economides, M. J., R. E. Oligney, and A. S. Demarchos, "Natural Gas: The Revolution is Coming," *J. Pet. Technol.*, **53**, 64 (2001).

Glew, D. N., and N. S. Rath, "Variable Composition of the Chlorine and Ethylene Oxide Clathrate Hydrates," *J. Chem. Phys.*, **44**, 1710 (1966).

Glew, D. N., "Aqueous Nonelectrolyte Solutions. Part XVIII. Equilibrium Pressures of Two Methane Hydrates with Water. Formulae and Dissociation Thermodynamic Functions for the Structures I and II Methane Hydrates," *Can. J. Chem.*, **80**, 418 (2002).

Handa, Y. P., "Calorimetric Studies of Laboratory Synthesized and Naturally Occurring Gas Hydrates," AIChE Meeting Miami Beach, FL (1986).

Huo, Z., M. D. Jager, K. T. Miller, and E. D. Sloan, Jr., "Ethylene Oxide Hydrate Non-Stoichiometry: Measurements and Implications," *Chem. Eng. Sci.*, **57**, 705 (2002).

Hyndman, R. D., J. P. Foucher, M. Uamano, and A. Fisher, "Deep Sea Bottom-Simulating-Reflector: Calibration of the Base of the Hydrate Stability Field as Used for Heat Flow Estimates," *Earth Planet. Sci. Lett.*, **109**, 289 (1992).

Jager, M. D., "High Pressure Studies of Hydrate Phase Inhibition Using Raman Spectroscopy," PhD Thesis, Colorado School of Mines, Golden, CO (2001).

Kobayashi, R., and D. L. Katz, "Methane Hydrate at High Pressure," *Trans AIME*, **186**, 66 (1949).

Kvenvolden, K. A., "Methane Hydrate—A Major Reservoir of Carbon in the Shallow Geosphere?" *Chem. Geol.*, **71**, 41 (1988).
Kvenvolden, K. A., and D. Lorenson, "The Global Occurrence of Natural Gas Hydrates," in *Natural Gas Hydrates*, C. K. Paull and W. P. Dillon, eds., American Geophysical Union, Washington, DC (2001).
Massalski, T. B., H. Okamoyo, P. R. Subramanian, and L. Kacprzak, eds., *Binary Alloy Phase Diagrams*, 2nd ed., ASM International, Materials Park, OH (1990).
Sloan, E. D., *Clathrate Hydrates of Natural Gases*, 2nd ed., Dekker, New York (1998).
Stern, L. A., S. H. Kirby, and W. B. Durhan, "Peculiarities of Methane Clathrate Hydrate Formation and Solid-State Deformation, Including Possible Superheating of Water Ice," *Science*, **273**, 1843 (1996).
Subramanian, S., "Measurements of Clathrate Hydrates Containing Methane and Ethane Using Raman Spectroscopy," PhD Thesis, Colorado School of Mines, Golden, CO (2000).
Subramanian, S., R. A. Kini, S. F. Dec, and E. D. Sloan, "Evidence of Structure II Hydrate Formation from Methane + Ethane Mixtures," *Chem. Eng. Sci.,* **55**, 1981 (2000).
Subramanian, S., and E. D. Sloan, "Solubility Effects on Growth and Dissolution of Methane Hydrate Needles," *Proc. Int. Conf. Gas Hydrates*, Yokohama, Japan, p. 856, (icgh@mori.mech.keio.ac.jp) (2002).
Udachin, K. A., C. I. Ratcliffe, and J. A. Ripmeester, "Proc., International Conf. on Gas Hydrates, Yokohama, Japan, p. 604 (2002).

Manuscript received May 21, 2002, and revision received Nov. 12, 2002.